View Article Online / Journal Homepage / Table of Contents for this issue
Dynamic Article Links

Soft Matter

Cite this: *Soft Matter*, 2011, **7**, 6973

www.rsc.org/softmatter

**PAPER**

# Aqueous phase behaviour of choline carboxylate surfactants—exceptional variety and extent of cubic phases†

**Regina Klein,[a] Gordon J. T. Tiddy,[b] Eva Maurer,[a] Didier Touraud,[a] Jordi Esquena,[c] Olivier Tache[d] and Werner Kunz*[a]**

***Received 21st January 2011, Accepted 24th May 2011***
**DOI: 10.1039/c1sm05108c**

Choline carboxylate surfactants are powerful alternatives to the well-known classical alkali soaps, since they exhibit substantially increased water solubility while maintaining biocompatibility, in contrast to simple quaternary ammonium ions. In the present study, we report the aqueous binary phase diagrams and a detailed investigation of the lyotropic liquid crystalline phases formed by choline carboxylate surfactants (ChC*m*) with chain lengths ranging from $m = 12$–18 and at surfactant concentrations of up to 95–98 wt%. The identification of the lyotropic mesophases and their sequence was achieved by the penetration scan technique. Structural details are elucidated by small-angle X-ray scattering (SAXS). The general sequence of mesophases with increasing soap concentration was found to be as follows: micellar ($L_1$), discontinuous cubic ($I_1$), hexagonal ($H_1$), bicontinuous cubic ($V_1$) and lamellar ($L_\alpha$). The main difference to the phase behavior of alkali soaps or of other mono-anionic surfactants is the appearance and large extent of a discontinuous cubic phase with two or even more different symmetries. The obtained phase diagrams further highlight the extraordinarily high water solubility of ChC*m* soaps. Finally, structural parameters of ChC*m* salts such as the cross-sectional area at the polar–nonpolar interface are compared to those of alkali soaps and discussed in the terms of specific counterion binding and packing constraints.

Published on 29 June 2011. Downloaded by Universitaetsbibliothek Regensburg on 21/07/2016 07:10:17.

## Introduction

In a previous study, we introduced choline (shown in Fig. 1) as a beneficial counterion of fatty acid soaps.[1] Compared to alkali soaps, choline carboxylate surfactants are featured by considerably lower Krafft points (the temperature above which ionic surfactants form micelles and dissolve well). For instance, the replacement of sodium by choline in palmitate (C16) salts brings about a Krafft point reduction from 60 °C down to 12 °C.[1,2] Simple quaternary ammonium ions (like tetrabutylammonium) are indeed also capable of lowering the Krafft temperatures of fatty acid salts,[3] but they suffer from their toxicological impact.[4–7] By contrast, the use of choline as a quaternary ammonium ion of biological origin sustains biocompatibility.[8–10]

The substantial decrease in the Krafft point observed with choline as counterion was explained on the basis of two contributing factors, namely by the hindrance of a regular crystalline packing by the bulky choline ion, which is most probably the main driving force, and by a weak counterion to headgroup binding.[1,11] Regarding their self-assembly behaviour, choline soaps were found to behave very akin to alkali soaps in the low concentration region with respect to critical micellization concentrations (*cmc*'s). In fact, measured *cmc* values coincided nearly exactly with those of the corresponding alkali salts.[1] These findings inevitably raise the question in which manner choline carboxylates self-assemble at higher concentrations. This is not only of fundamental interest but also important for industrial applications.[12]

The first binary aqueous phase diagrams of sodium and potassium soaps were established by McBain, Vold and coworkers.[2,13,14] Later, Madelmont and Perron refined those of sodium laurate (NaC12) and myristate (NaC14) by means of

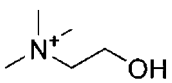


**Fig. 1** Molecular structure of choline.

[a]*Institute of Physical and Theoretical Chemistry, University of Regensburg, 93040 Regensburg, Germany. E-mail: werner.kunz@chemie.uni-regensburg.de; Fax: +49 941 943 4532; Tel: +49 941 943 4044*
[b]*Department of Chemical Engineering, University of Manchester, Manchester, M60 1QD, UK*
[c]*Institute for Advanced Chemistry of Catalonia, CSIC, Barcelona, Spain*
[d]*Laboratoire Interdisciplinaire sur l'Organisation Nanométrique et Supramoléculaire CEA/IRAMIS, CEA Saclay, 91191 Gif sur Yvette, France*

† Electronic supplementary information (ESI) available: Density data and calculation of the molar volumes of ChC*m* surfactants, further penetration scan images, experimental X-ray setups, SAXS diagrams, listed X-ray diffraction data and details on the lattice calculations. See DOI: 10.1039/c1sm05108c.

View Article Online

Published on 29 June 2011. Downloaded by Universitaetsbibliothek Regensburg on 21/07/2016 07:10:17.

differential thermal analysis.[15] Luzzati, Spegt and Skoulios are just a few further names of authors who investigated in depth the aqueous phase behaviour of alkali soaps and resolved the detailed structure of the mesophases by thorough X-ray studies.[16–21] The basic phase behaviour is similar for all alkali carboxylate surfactants.[22] The characteristic sequence of mesophases occurring with increasing surfactant concentration is: micellar solution $L_1$, normal hexagonal $H_1$, bicontinuous cubic $V_1$ (which may be accompanied or replaced by one or two intermediate phases), and lamellar $L_\alpha$. In aqueous micellar solutions, all soaps undergo a transition from spherical to rod-like micelles when their concentration is increased.[23,24] As a consequence, normal hexagonal $H_1$ is the first liquid crystalline phase to be formed. This has been shown to apply also for carboxylate surfactants with big organic counterions like alkyl amines or quaternary ammonium ions.[25,26] In turn, discontinuous cubic phases ($I_1$), which are typically located between $L_1$ and $H_1$ and consist of discrete, mostly spherical micelles arranged in a cubic lattice, have to our knowledge not been reported to date for any binary aqueous mono-anionic surfactant system.[27,28] Such phases are indeed known for divalent anionic,[29] zwitterionic,[30] non-ionic[31,32] and even mono-cationic surfactants with highly dissociated counterions (*e.g.* alkyltrimethylammonium chloride),[30] due to an increased effective area per headgroup $a_o$. Moreover, it should be noted that such cubic phases have also been identified in ternary or more complex mixtures of anionic surfactants.[33,34]

Herein, we shed light on the influence of counterion binding on micellar shape and the formation of lyotropic liquid crystals in choline carboxylate systems. To that end, the binary aqueous phase diagrams of choline soaps (ChC*m*) are presented for chain lengths of $m = 12$–18 and a temperature range of 0–90 °C. The various mesophases and their sequence were identified first by the penetration scan technique using optical polarizing microscopy. Subsequently, the exact phase boundaries were determined visually between crossed polarizers. Finally, structural details of the lyotropic liquid crystalline phases were elucidated by small-angle X-ray scattering (SAXS) measurements performed for surfactant concentrations up to 95–98 wt%.

## Results and discussion

### Penetration scans

The penetration scan method, as described in detail by Lawrence,[35] is a straightforward technique to obtain information on the mesophases formed by a surfactant in water. Thereby, the various liquid crystals with their different characteristic textures are observed in the form of distinct rings along increasing surfactant concentration towards the center of the sample.

Fig. 2 shows a penetration scan image of ChC12 at 20 °C. When passing to higher surfactant concentrations, the following sequence of mesophases can be identified: micellar ($L_1$), discontinuous cubic ($I_1'$ and $I_1''$), hexagonal ($H_1$), bicontinuous cubic ($V_1$), and a partially birefringent solid region. A lamellar phase ($L_\alpha$) could not be detected before 62 °C. Generally, discontinuous cubic phases can be distinguished in a penetration scan by their high viscosity (obvious when slightly pushing the sample) as well as their isotropy and refractive index discontinuity. The

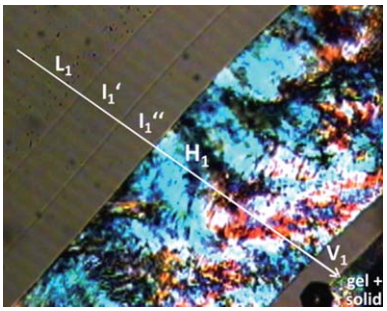


**Fig. 2** Penetration scan of ChC12 at 20 °C acquired at 100× magnification between half-crossed polarizers, showing the following sequence of the formed mesophases: $L_1$, $I_1'$ and $I_1''$, $H_1$, $V_1$ and a gel + solid region. The discontinuous cubic phases $I_1'$ and $I_1''$ can be identified by their isotropy, high viscosity and refractive index discontinuities (dark lines).

penetration scan of ChC12 clearly indicates the presence of two different discontinuous cubic phases, labelled $I_1'$ and $I_1''$, with almost equal extent. The $H_1$ phase can be recognized by its characteristic optical texture,[36] while the bicontinuous cubic $V_1$ phase is isotropic and highly viscous. The solid region was found to be partially birefringent and exhibits, in contrast to a lamellar phase, high viscosity. Therefore, we suggest that it corresponds to a mixture of a gel ($L_\beta$) and a solid phase, as observed previously for potassium and higher alkali soap derivatives.[22,37] The phase behaviour of the gel or coagel region can be rather complex since an equilibrium state is often difficult to attain.[20,38] Therefore, we will focus in the following on the liquid crystalline phases.

The general sequence of liquid crystals observed for ChC12 was confirmed also for the longer-chain choline carboxylates, including the existence of two $I_1$ phases. Only ChC18 differs slightly from the other homologues as the $I_1''$ phase disappears at around 55 °C, while for $m = 12$–16 both cubic phases are present over the entire temperature range investigated.

Fig. 3 shows another example of a penetration scan, which illustrates the more concentrated surfactant region of ChC16 at 61 °C. The phases occurring towards higher soap concentration are assigned to $H_1$, $V_1$, $L_\alpha$ and $L_\beta$. Further penetration scan images acquired for the different choline soaps at various temperatures can be found in the ESI†.

### Binary phase diagrams

From the penetration scans, it can be deduced that the aqueous phase behaviour of choline soaps is characterized by an

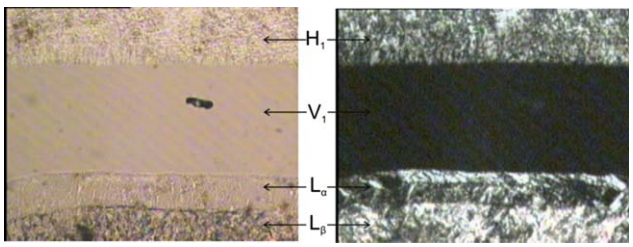


**Fig. 3** Penetration scan of ChC16 at 61 °C with non-crossed (left) and crossed (right) polarizers at 100× magnification, visualizing the formed mesophases in the more concentrated surfactant region.

 This journal is © The Royal Society of Chemistry 2011

View Article Online

Published on 29 June 2011. Downloaded by Universitaetsbibliothek Regensburg on 21/07/2016 07:10:17.

alternating sequence of isotropic and anisotropic liquid crystals. Consequently, the exact phase boundaries can be identified by inspecting samples with distinct concentrations between crossed polarizers at varying temperatures. In turn, the boundary between $I_1'$ and $I_1''$ must be estimated based on the penetration scans and SAXS data. The $T_C$ line, *i.e.* the boundary between crystalline and "melted" paraffinic chains, was determined visually by detecting the temperature where the samples become transparent and was further confirmed by DSC measurements for selected samples (data not shown). Fig. 4 shows the resulting aqueous binary phase diagrams of ChC*m* surfactants for $m = 12$–18 and $T = 0$–90 °C. The accuracy of the phase boundaries is estimated to be within ±1 wt% and ±1 °C. Higher temperatures have not been investigated due to the problem of thermal decomposition. Consisting of organic material only, choline soaps start to become dark when heated over 90 °C for longer periods.

All phase transitions appear to be of first order, as a small two-phase region could be detected in each case, which is distinctly larger in-between $I_1''$ and $H_1$ than for the other transitions. Nevertheless, the two-phase regions are in general relatively small and thus suggest high purity of the used surfactants.

The Krafft boundary shifts as expected to higher temperatures with growing chain length. At around 95 wt% soap in water all choline surfactants show a pronounced increase in $T_C$. However, an unexpected feature concerning the Krafft boundary line is the increase of $T_C$ at surfactant concentrations lower than 5–10 wt% in the phase diagrams of ChC16 and ChC18. Similar observations have been reported by McBain *et al.* for potassium soaps and were explained by the hydrolysis of the fatty acids, which is more prominent in dilute solutions.[13] Moreover, the degree of hydrolysis also depends strongly on the alkyl chain length. Kanicky *et al.* showed that the apparent p$K_a$ value increases with the chain length from ~7.5 for C12 to 10.15 for C18.[39–41] In this regard, the dilute region of ChC16 and ChC18 does not represent a true binary system. On the other hand, adding an extra amount of choline base to suppress fatty acid hydrolysis would likewise not result in a true binary system, since an excess of choline ions would be present in this case.

Fig. 4 further visualizes that choline soaps start forming liquid crystals at around 26–29 wt% surfactant in water. The onset of the $I_1'$ phase is thereby displaced slightly to lower concentrations with growing chain length. All liquid crystalline phase boundaries shift to lower soap concentrations for longer alkyl chains. This effect is most distinct for $H_1$. The $I_1$ phase region shrinks with increasing *m*, extending for ChC12 over about 18 wt% while for ChC18 only over roughly 3 wt%. Also, the $V_1$ region becomes smaller at higher *m* values, whereas the $H_1$ and $L_\alpha$ phase domains expand simultaneously. Apparently, phases of high curvatures, namely the cubic phases, become less favoured the longer the alkyl chain is. This is well in line with literature and the known tendency of longer alkyl chain derivatives to form less curved surfactant aggregates.[38,42,43]

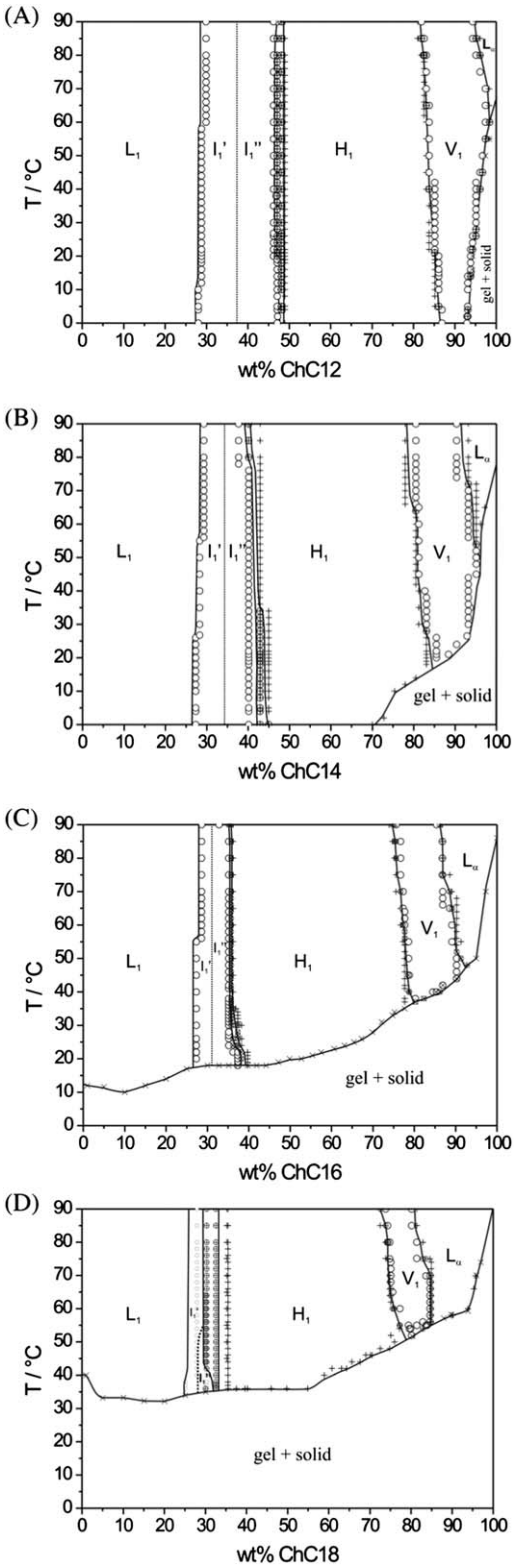


**Fig. 4** Binary aqueous phase diagrams of ChC*m* surfactants between 0 °C and 90 °C for $m = 12$ (A), $m = 14$ (B), $m = 16$ (C) and $m = 18$ (D). Experimental data near the phase boundaries were determined visually between crossed polarizers as isotropic (○), biphasic (⊕) and anisotropic (□).

## Comparison to alkali soaps

Sodium and potassium soaps form liquid crystals ($H_1$) at comparable concentrations as choline carboxylates (20–30 wt% surfactant in water depending on the chain length).[2,12,14] The

View Article Online

Published on 29 June 2011. Downloaded by Universitaetsbibliothek Regensburg on 21/07/2016 07:10:17.

found basic phase behaviour of choline soaps is generally also similar to the alkali homologues.[2,12,25] However, there are some important deviations:

(1) The studied choline soaps exhibit two distinct $I_1$ phases between $L_1$ and $H_1$.

(2) Ch*Cm* salts form a single $V_1$ phase up to $m = 18$ and do not display intermediate phases. By contrast, the $V_1$ phase is fully replaced by intermediate phase(s) for sodium at $m = 12$ and for potassium soaps at $m = 14$.[44]

(3) The $L_\alpha$ phase region of Ch*Cm* surfactants is considerably smaller than observed for simple soaps, even if compared to large alkali ions such as cesium.[23] Sodium and potassium carboxylates, for instance, typically form a lamellar phase between 60 and 65 wt%.[2,12]

(4) The Krafft boundary of choline carboxylates is shifted to considerably lower temperatures relative to alkali soaps.[2,13,15]

When compared to their choline counterparts, alkali carboxylate surfactants prefer phases of lower curvature, to a greater extent the smaller the counterion ($Li^+ > Na^+ > K^+ > Rb^+ > Cs^+$). This trend reflects the known order of counterion binding and becomes further manifest in the Krafft point reduction of carboxylate soaps towards bigger alkali ions.[11,45,57,58] In this context, choline can be regarded as a simple continuation of the alkali series. The bulky, highly dissociated choline counterion induces a large cross-sectional headgroup area $a_S$ and hence provokes two outstanding characteristics in the aqueous phase behaviour: a low Krafft boundary up to very high concentrations and a discontinuous cubic phase which extends over a wide concentration region.[46] For instance, ChC12 shows no Krafft phenomenon down to 0 °C up to 93 wt% surfactant in water. As opposed to that, the Krafft temperature of 90 wt% NaC12 is 127 °C (or 195 °C for KC12).[14] Discontinuous cubic phases have to date been observed for example for mono-cationic surfactants like alkyltrimethylammonium chlorides with chain lengths up to $m = 14$,[33,59] but not for mono-anionic surfactants in binary mixtures with water. Strikingly, choline soaps even show two distinct $I_1$ phases in water, which has previously only been reported for non-ionic,[35,60] zwitter-ionic[33] and divalent surfactants.[32]

## SAXS data and analysis

In the following, SAXS analyses of each liquid crystalline phase (recorded in concentration steps of ≤2.5 to 5.0 wt%) are presented in order to provide further insight into structural details of the phases and confirm their assignment.

### Discontinuous cubic $I_1'$

Penetration scans indicate that at least two differently structured $I_1$ phases occur in the systems. Exemplary two-dimensional X-ray patterns acquired from ChC12 are displayed in Fig. 5. These show, with increasing surfactant concentration, a single $I_1'$ phase (30.0–35.1 wt%), the coexistence of $I_1'$ and $I_1''$ (37.9 wt%), a pure $I_1''$ phase (40.1–45.0 wt%), a biphasic pattern of $I_1''$ and $H_1$ (47.2 wt%), and eventually a single $H_1$ phase (49.7 wt%).

It is well known that cubic phases often grow to large monocrystals, thus effecting rather spotty X-ray patterns instead of rings.[28,47] This applies in particular for the $I_1'$ phase, while in $I_1''$ homogeneous rings become more and more established.

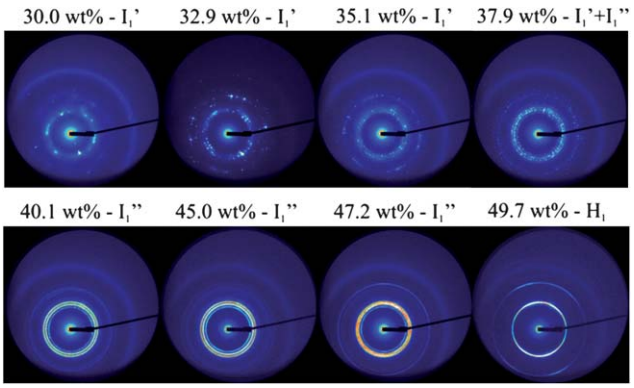


**Fig. 5** Two-dimensional X-ray patterns of the system ChC12/$H_2O$ at 25 °C at surfactant concentrations ranging from 30.0–49.7 wt% ChC12, showing single and biphasic patterns of the discontinuous cubic phases $I_1'$ and $I_1''$ and the hexagonal phase $H_1$.

Fig. 6(A) shows a radially averaged scattering profile of the $I_1'$ phase of ChC12 (X-ray spectra of $I_1'$ for both, different chain lengths and concentrations, are given in the ESI†). Several attempts were made to solve the structure, but neither a primitive nor a face- (*fcc*) or body-centred (*bcc*) lattice describe the data adequately well. In turn, $I_1''$ could be clearly assigned to a *Pm*3*n* structure (see below). Therefore, particular effort was spent trying space groups like *Im*3*m*, *Fm*3*m* and *Fd*3*m*, since they often accompany a *Pm*3*n* lattice.[27,28,32] Although several reflections match to these space groups, some peaks always remained non-indexed. The best agreement was achieved when using the cubic structure described by Clerc in 1996,[48] which consists of two spherical micelles per unit cell arranged in hexagonal compact structure (*hcp*) with $P6_3/mmc$ symmetry.[48,49] The dashed lines inserted to the spectrum in Fig. 6(A) show the attempt to assign $I_1'$ to this structure (see the ESI† for details on calculations). It is evident that the experimental spectrum is still not properly fitted.

A possible reason for the difficulties in finding the right space group could be that the *hcp* and *fcc* packing are energetically closely related.[50] Consequently, the relative stability of these two phases strongly depends on nucleation and growth kinetics.[49] The fact that they are likely to coexist may account for the result that $I_1'$ cannot be simply assigned to a single structure. However, since we measured samples of different concentrations and chain lengths and could not detect noticeable differences upon ageing for years, we assume that the X-ray pattern of $I_1'$ reliably represents thermodynamic equilibrium of the samples. Another problem in indexing $I_1'$ may arise due to the formation of large monocrystals. By simple radial averaging over the spots, substantial information on different domains of structures might get lost. Hence, a feasible means to further analyze the system could be to rotate the sample or to measure monodomains, which was unfortunately not possible with the used setups.

### Discontinuous cubic phase $I_1''$

As evidenced by Fig. 6, the $I_1''$ phase of ChC12 could be indexed properly by a *Pm*3*n* lattice. Equally unambiguous assignments

 This journal is © The Royal Society of Chemistry 2011

View Article Online

Published on 29 June 2011. Downloaded by Universitaetsbibliothek Regensburg on 21/07/2016 07:10:17.

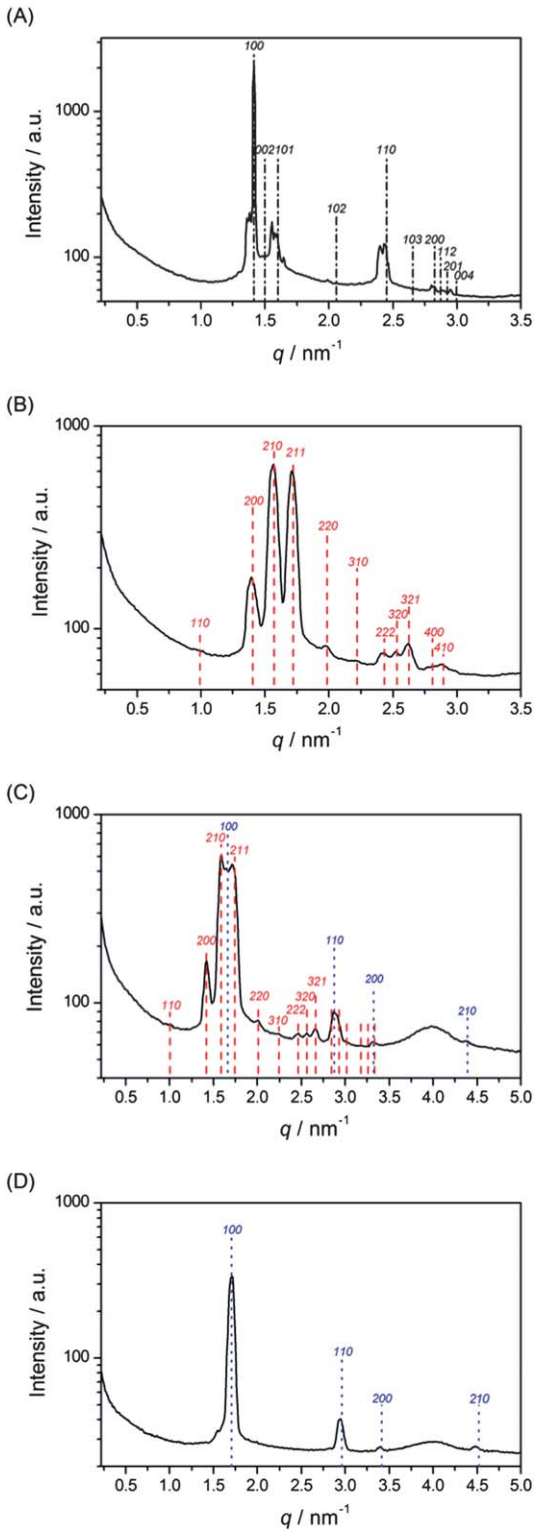


**Fig. 6** Radially averaged SAXS profiles of ChC12 at 25 °C and surfactant concentrations of (A) 35.1, (B) 40.1, (C) 47.2, and (D). 49.7 wt %. Vertical lines mark the positions and *Miller* indices of peaks expected for a $P6_3/mmc$ (-·-), $Pm3n$ (–) and $H_1$ (···) structure. Patterns correspond to (A) a single $I_1'$ phase tentatively assigned to a $P6_3/mmc$ structure, (B) a single $I_1''$ with $Pm3n$ symmetry, (C) a biphasic region of $I_1''$ ($Pm3n$) and $H_1$, and (D) a pure $H_1$ phase. Note that the bump around $q = 4$ nm$^{-1}$ stems from Kapton foil.

were possible also for the other chain lengths, with up to 12 identified peaks (see the ESI† for further diffraction data). Cubic phases with $Pm3n$ symmetry, located between $L_1$ and $H_1$, have been reported in earlier studies on binary and ternary surfactant systems.[28,47,51,52] However, the detailed structure of $Pm3n$ has in the past been the object of debates.[27,28,53–56] Eventually, NMR-diffusion measurements[53] as well as detailed X-ray[57] and freeze-fracture electron microscopy studies[58] support the model of Charvolin and Sadoc, who proposed a structure comprising two spherical and six disc-shaped (oblate) micelles per unit cell without any dynamic disorder.[59] Accordingly, structural parameters such as the micellar radius or the effective cross-sectional headgroup area can at this point not be calculated in a straightforward way and would require more efforts such as mapping of the electron density.

The unit cell parameters $a$ determined for $I_1''$ range from about 90 Å to 125 Å (Table 1) and are reasonable with respect to other systems such as aqueous dodecyltrimethylammonium chloride.[47] The addition of two $CH_2$ groups increases $a$ on average by about 15–20 Å. This cannot be simply explained by the length of two $CH_2$ groups (2.5 Å × 4 = 10 Å). The increase of $a$ with growing chain lengths is most probably also caused by the larger dimensions of oblate micelles.

In a rough approximation, the micelle aggregation number $N_{agg}$ can be calculated under the assumption of eight spherical micelles in the unit cell according to eqn (1).

$$N_{agg} = (V_{unit\ cell}\Phi_s/V_s)/8 \quad (1)$$

The resulting values (Table 1) vary from 71 for ChC12 up to 139 for ChC16, and are thus on a reasonable order of magnitude. As expected, $N_{agg}$ increases with the chain length and the concentration.

### Hexagonal phase $H_1$

At around 35–50 wt% (depending on $m$), choline soaps start forming a hexagonal phase, which can be identified by up to 4–5 reflections (see Fig. 6(D) and Table S6 in the ESI†). For the $Pm3n$–$H_1$ transition, several groups suggested an epitaxial relationship which facilitates the conversion of the 211 plane in the cubic phase into the 100 plane of the hexagonal lattice.[60,61] As shown by the biphasic spectrum of 47.2 wt% ChC12 (*cf.* Fig. 6 (C)), the 100 spacing of $H_1$ is centred exactly in the middle between the 210 and 211 reflection of $Pm3n$. Moreover, we could not detect any systematic change in the relative intensity of the 211 spacing of $Pm3n$ towards higher soap concentrations. In this sense, it seems as if choline soaps do not follow the proposed transition mechanism.

The interlayer spacing $d$ of $H_1$ decreases linearly with the surfactant concentration (Fig. 7(A)), which can be interpreted by a closer packing of the micellar cylinders. Corresponding changes in the lipophilic radius $r_L$ (derived by eqn (4)) are outlined in Fig. 7(B) for the different $m$ values. As expected, $r_L$ increases in an approximately linear fashion with the concentration. The determined slopes ($\Delta r_L/\Delta\Phi_L = 4.0$–$4.8$) are within the limits of experimental error equal for all homologues, indicating that the micellar radii grow in a similar manner. In all cases, $r_L$ is around 10–20% smaller than the respective fully extended alkyl chain $l_{max}$ (Table 4), which agrees well with the

View Article Online

Published on 29 June 2011. Downloaded by Universitaetsbibliothek Regensburg on 21/07/2016 07:10:17.

**Table 1** Unit cell parameters $a$ of the $Pm3n$ structure detected for the $I_1''$ phase of ChC$m$ salts up to $m = 16$ at 25 °C, with corresponding estimated aggregation numbers $N_{agg}$. 37.9 wt% ChC12 and 34.9 wt% ChC14 are biphasic samples of $I_1'$ and $I_1''$, while 47.2 wt% ChC12 belongs to the two-phase region of $I_1''$ and $H_1$

| | ChC12 | | | | ChC14 | | | ChC16 |
|---|---|---|---|---|---|---|---|---|
| wt% | 37.9 | 40.1 | 45.0 | 47.2 | 34.9 | 37.4 | 40.9 | 34.8 |
| $a$/Å | 91.3 ± 0.5 | 89.9 ± 0.3 | 88.8 ± 0.2 | 88.4 ± 0.4 | 105.8 ± 1.1 | 106.1 ± 1.0 | 106.7 ± 1.2 | 124.9 ± 0.8 |
| $N_{agg}$ | 70.9 | 71.4 | 77.4 | 79.8 | 92.7 | 100.1 | 111.1 | 139.4 |

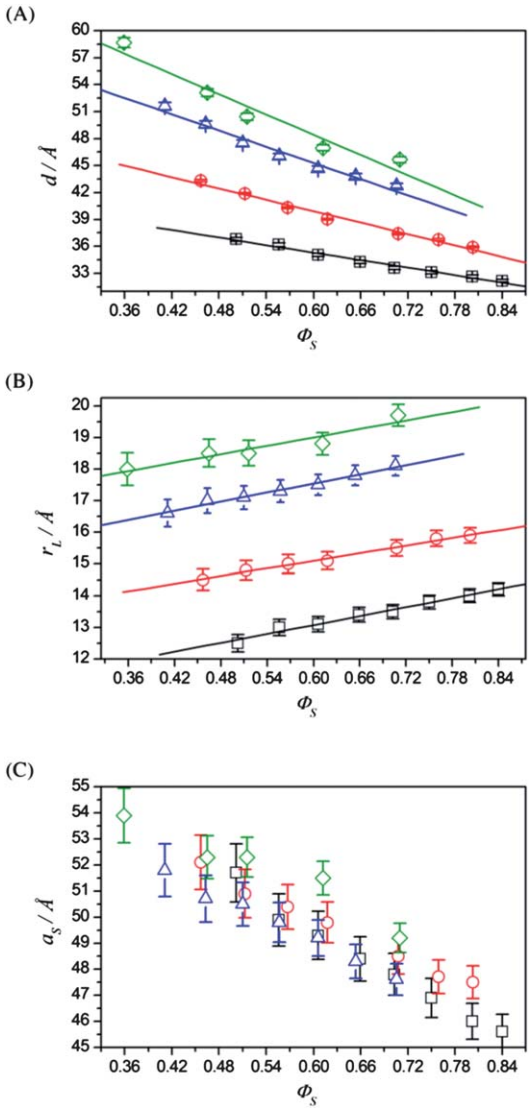


**Fig. 7** The interlayer spacing $d$ (A), the radius of the lipophilic part $r_L$ (B) and the cross-sectional area at the polar–nonpolar interface $a_S$ (C) outlined as a function of $\Phi_S$ for the hexagonal phase of ChC$m$ soaps (ChC12 (□), ChC14(○), ChC16 (△) and ChC18 (◇)) ($T$= 25 °C for $m$ = 12–16, and $T$= 50–60 °C (see ESI†) for $m$ = 18). The error bars were calculated assuming uncertainties of $\Delta q = 0.01$ nm and $\Delta\Phi_L = 0.01$.

literature.[38] Upon addition of two $CH_2$ groups, $r_L$ increases at a given volume fraction by about 1.5–2.4 Å, which complies with reported values.[22,62]

The effective cross-sectional area at the polar–nonpolar interface $a_S$ (derived by eqn (5)) is reproduced as a function of the surfactant volume fraction for the different $m$ values in Fig. 7(C). Only ChC18 tends to slightly larger $a_S$ values, while those of $m$ = 12–16 are more or less equal. This can probably be attributed to the higher temperatures chosen for measuring the ChC18 data due to its higher Krafft point. With growing surfactant concentration, $a_S$ decreases from about 52 Å$^2$ to 46 Å$^2$, finally reaching the limit at which the molecules can be packed in cylinders.

To enable a comparison of our results to data reported for the sodium and potassium homologues, values cited in literature were recalculated in order to obtain the cross-sectional area at the polar–nonpolar instead of the surfactant–water interface.[63] Given the high Krafft temperatures of Na- and K-carboxylates, documented values were determined at 86 °C.[63] However, for ionic surfactants the influence of temperature on structural parameters is rather small. When considering similar volume fractions (~50% surfactant), the following tendency of $a_S$ is obtained for $m$ = 12:

$$\text{NaC12}\ (a_S = 46.7\ \text{Å}^2)^{63} < \text{KC12}\ (a_S = 47.3\ \text{Å}^2)^{63} \ll \text{ChC12}\ (a_S = 51.7\ \text{Å}^2)$$

This is well in line with the increasing size of the counterions and the concurrent decrease of counterion–headgroup association.[11,45] Moreover, it confirms the idea by Zemb *et al.* that ionic micelles are adequate models for quantifying specific ion effects.[46]

### $H_1$–$V_1$ boundary: intermediate phase?

Close to the phase boundary between $H_1$ and $V_1$, additional reflections appear in the X-ray patterns which can be allocated neither to $H_1$ nor, apparently, to $V_1$ (which belongs to the $Ia3d$ space group, see below). These peaks are unlikely to arise from insufficient equilibration, since four month-old samples give the same scattering profiles as those measured after one week.

As already mentioned, several intermediate phases located between $H_1$ and $V_1$ or $H_1$ and $L_\alpha$ have been identified for alkali soaps or other mono-ionic surfactants. Luzzati *et al.* described an intermediate phase with complex hexagonal structure,[18,20] which is known today as *ribbon* phase with centred rectangular symmetry (*cmm*).[64] This structure exhibits peak ratios typical for a hexagonal lattice, but with much larger lattice dimensions and more irregular peak intensities.[18,20] The additional peaks observed in the $H_1/V_1$ region match the Bragg spacing ratios of a two-dimensional hexagonal lattice, as shown exemplarily for ChC16 in Fig. 8 (see the ESI† for further details and X-ray data).

The detected $d$ spacings are indeed larger than those of $H_1$, but by far not to such an extent as reported by Luzzati *et al.*, who

 This journal is © The Royal Society of Chemistry 2011

View Article Online

Published on 29 June 2011. Downloaded by Universitaetsbibliothek Regensburg on 21/07/2016 07:10:17.

observed almost two times higher $d$ values in the intermediate region than in $H_1$.[18] Moreover, common intermediate phases are of anisotropic nature, which is clearly in conflict with the isotropy noticed for the samples in this concentration regime. And beyond that, the penetration scans gave no evidence of an intermediate phase for any of the investigated choline soaps.

An alternative approach would be to index these additional peaks by another cubic lattice, namely $I4_132$,[65,66] which is a subgroup of *Ia*3*d* (see ESI†). However, reflections of fourth and fifth order ($d_{310}$ and $d_{222}$) are all missing in this case. Consequently, the complex hexagonal structure represents a better fit of the data, since the reflections could be assigned in increasing order without extinctions in-between them.

For the $H_1$–$V_1$ transition, Rancon and Charvolin suggested an epitaxial relationship between the 211 plane of *Ia*3*d* and the 100 plane of the hexagonal lattice.[60] Accordingly, 2 $d_{211}/\sqrt{3}$ of *Ia*3*d* should equal $d_{100}$ of $H_1$,[60] which however could not be confirmed by the present set of data. This either rules out an epitaxial relationship of $H_1$ and $V_1$ or in turn supports the existence of an additional phase between $H_1$ and $V_1$. At the moment, no unambiguous conclusions can be drawn on whether an intermediate phase, an additional cubic phase, or any extra phase at all exists between $H_1$ and $V_1$.

### Bicontinuous cubic phase $V_1$

In a bicontinuous cubic phase, the aggregates form a three-dimensional network extending throughout the sample. The structures formed are well described by *infinite periodic minimal surfaces* (IPMS),[28,67,68] *i.e.* surfaces whose mean curvature is zero at all points. Most commonly obtained in $V_1$ phases of lipid–water systems is the I*a*3*d* group, which corresponds to the "gyroid" (G) type surface, having a negative Gaussian interfacial curvature.[28,68] The $V_1$ phase of choline soaps also belongs to the *Ia*3*d* symmetry, as confirmed by up to six assigned reflections (see Fig. 9). As observed for $H_1$, the peaks are shifted to lower $d$ values when the surfactant concentration is increased and to higher $d$ values when longer alkyl chains are used (*cf.* Table 3). In the framework of the IPMS concept, the length of the lipophilic part and the area per surfactant headgroup cannot be calculated in a simple manner. However, the determined unit cell parameters $a$ (Table 2) are generally in the same order of magnitude as those of other mono-ionic surfactants.[19,27,69] Towards higher soap concentrations, $a$ decreases as the effective alkyl chain length is increased and the effective headgroup area diminished. Addition of two $CH_2$ groups enlarges reasonably the unit cell by about 5–10 Å.[22]

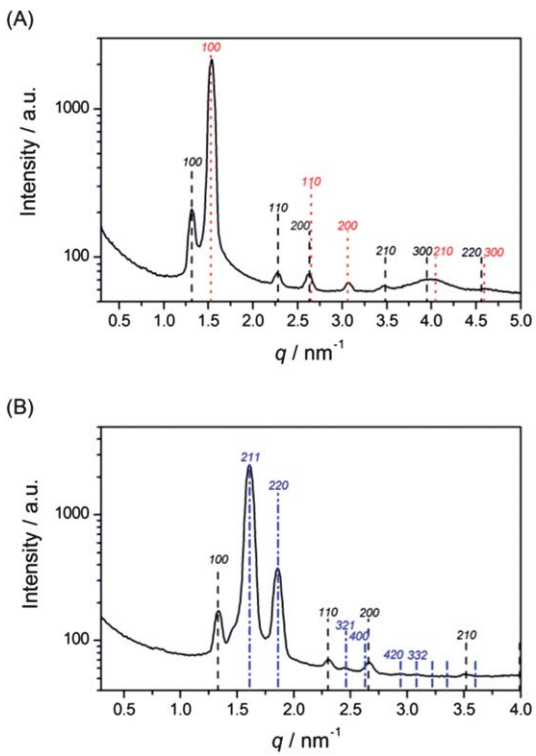


**Fig. 8** SAXS spectra of (A) 74.8 wt% ChC16 ($T$= 60 °C) and (B) 79.3 wt % ChC16 ($T$ = 50 °C), representing biphasic samples of a potential intermediate phase and $H_1$ (A) or, respectively, $V_1$ (B). Theoretical peak positions are indicated by the vertical lines with the corresponding *Miller* indices outlined above (complex hexagonal (–), $H_1$ (···) and *Ia*3*d* (-·-·)). The bump around $q = 4$ nm$^{-1}$ is due to the Kapton foil.

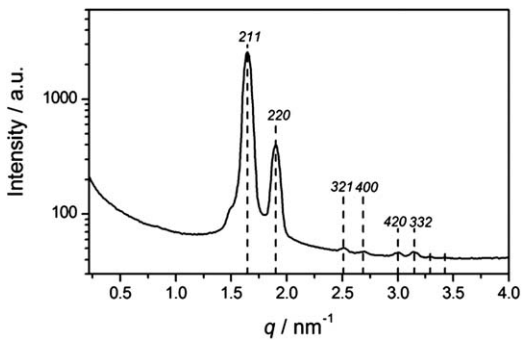


**Fig. 9** SAXS spectrum of $V_1$ of ChC16 (85.5 wt%, 50 °C), revealing *Ia*3*d* symmetry. The vertical lines mark the theoretical peak positions with the corresponding Miller indices outlined above.

**Table 2** Results of SAXS analyses for $V_1$ of ChC$m$ soaps with *Ia*3*d* structure, with the volume fraction of surfactant $\Phi_S$, the temperature $T$, the experimental $d$-values of the respective first order reflection and the unit cell parameter $a$. Samples of ChC12 up to 89.5 wt% as well as 79.3 wt % ChC16 and 75.7 wt% ChC18 are potentially biphasic as discussed in the text

| | wt% | $\Phi_S$ | $T$/°C | $d_{211}$/Å | $a$/Å |
|---|---|---|---|---|---|
| ChC12 | 86.9 | 0.871 | 25 | 31.1 | 76.2 ± 0.1 |
| | 89.5 | 0.897 | 25 | 30.8 | 75.6 ± 0.2 |
| | 91.5 | 0.916 | 25 | 30.4 | 74.6 ± 0.2 |
| | 94.0 | 0.941 | 25 | 30.2 | 74.0 ± 0.2 |
| | 97.5 | 0.975 | 60 | 29.0 | 71.1 ± 0.2 |
| ChC14 | 79.8 | 0.803 | 60 | 34.0 | 83.1 ± 0.1 |
| | 83.3 | 0.837 | 25 | 35.1 | 86.3 ± 0.5 |
| | 85.5 | 0.859 | 20 | 34.5 | 84.8 ± 0.3 |
| | 90.4 | 0.906 | 25 | 33.6 | 82.6 ± 0.3 |
| | 93.2 | 0.934 | 35 | 32.9 | 80.7 ± 0.3 |
| | 95.1 | 0.952 | 45 | 32.4 | 79.7 ± 0.4 |
| ChC16 | 79.3 | 0.800 | 50 | 39.0 | 95.8 ± 0.4 |
| | 85.5 | 0.860 | 50 | 38.1 | 93.4 ± 0.2 |
| | 89.3 | 0.897 | 50 | 37.6 | 92.1 ± 0.1 |
| ChC18 | 75.7 | 0.766 | 70 | 42.2 | 103.3 ± 0.3 |
| | 79.8 | 0.806 | 70 | 41.1 | 101.4 ± 0.4 |

View Article Online

Published on 29 June 2011. Downloaded by Universitaetsbibliothek Regensburg on 21/07/2016 07:10:17.

### Lamellar phase $L_\alpha$

The lamellar or "neat" phase, in which surfactants are arranged in bilayers, is the most common structure among all liquid crystals. This phase is not only of biological relevance with respect to cellular membranes, but also occurs in daily life products such as hand soaps. However, the region of $L_\alpha$ formed by choline soaps up to $m = 18$ is rather small. The results of SAXS analyses are summarized in Table 3, while corresponding diagrams are shown in the ESI†.

**Table 3** Structural parameters of the lamellar phase formed by ChC*m* soaps with $m = 14$–18, comprising the experimental *d*-values, the ratio of the lipophilic bilayer thickness $d_L$ and the all-*trans* alkyl chain length $l_{max}$, the difference of the surfactant length $r_S$ and the lipophilic half-length $r_L$ (representing the headgroup-counterion layer), and the thickness of the water layer $d_W$

| | wt% | $\Phi_S$ | $d_{100}$/Å | $(d_L/l_{max})$/Å | $(r_S - r_L)$/Å | $d_w$/Å |
|---|---|---|---|---|---|---|
| ChC14 | 95.1 | 0.952 | 29.4 | 1.03 | 4.7 | 1.4 |
| | 97.5 | 0.976 | 29.0 | 1.04 | 4.8 | 0.7 |
| ChC16 | 92.0 | 0.923 | 32.6 | 1.01 | 4.7 | 2.5 |
| | 94.0 | 0.942 | 32.2 | 1.02 | 4.7 | 1.9 |
| | 95.3 | 0.955 | 32.1 | 1.03 | 4.7 | 1.4 |
| | 97.5 | 0.976 | 31.7 | 1.04 | 4.8 | 0.8 |
| ChC18 | 85.7 | 0.863 | 36.1 | 0.97 | 4.5 | 4.9 |
| | 90.2 | 0.906 | 35.5 | 1.00 | 4.6 | 3.3 |
| | 96.0 | 0.962 | 34.9 | 1.04 | 4.8 | 1.3 |

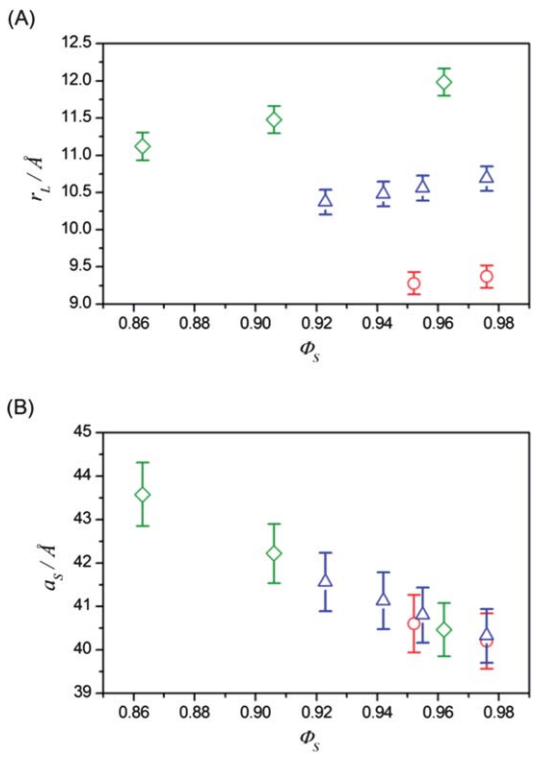


**Fig. 10** Half-length of the lipophilic bilayer $r_L$ (A) and the cross-sectional area at the polar–nonpolar interface $a_S$ (B) in the lamellar phase of ChC*m* surfactants plotted as a function of volume fraction surfactant $\Phi_S$ (ChC14 (○), ChC16 (△) and ChC18 (◇)).The error bars were calculated assuming uncertainties of $\Delta q = 0.01$ nm and $\Delta\Phi_L = 0.01$.

As in the other liquid crystals, reflections shift to lower *d* values with increasing surfactant concentrations due to a closer packing of the bilayers, and to larger *d* values for longer alkyl chains (Table 3). The half-length of the lipophilic bilayer $r_L$ increases more or less linearly with the concentration (Fig. 10(A)). Thereby, $r_L$ is on average around 50% smaller than $l_{max}$ for all investigated chain lengths. In other words, the total bilayer thickness equals approximately 1.0 $l_{max}$ for all *m* values, which indicates high disorder of the paraffinic chains.[46] The water layer $d_w$ (Table 3) is very small due to the high soap concentrations. The headgroup and counterion layer ($r_S - r_L$) cover about 4.7 Å in thickness, irrespective of the concentration and the chain length. This appears quite small when noting that the length of an extended choline ion is about 8 Å. A possible explanation for this finding is that choline is arranged in the layer with its long axis perpendicular to the director plane.

As in $H_1$, the effective cross-sectional area $a_S$ is more or less equal for different *m* values and decreases with growing surfactant concentration, from about 44 Å$^2$ to 40 Å$^2$ (Fig. 10(B)). Again, choline surfactants show significantly larger $a_S$ values than alkali soaps. For instance, a headgroup area of $a_S = 34.2$ Å$^2$ was reported for the lamellar phase of KC18 at 82.3 wt% and 86 °C.[63] For comparison, ChC18 requires 43.6 Å$^2$ at 85.7 wt% and 70 °C. This confirms the reported notion of a low counterion to headgroup association for carboxylate systems with large (or "soft") counterions.[45,70]

## Conclusions

Aqueous binary phase diagrams of ChC*m* soaps with $m = 12$–18 have been established over a temperature range of 0–90 °C with the help of polarizing microscopy and small-angle X-ray scattering. In analogy to alkali soaps, choline carboxylates start forming liquid crystals at around 26–29 wt%. Although the basic phase behaviour of ChC*m* salts is similar to that of other monoanionic surfactants, some outstanding characteristics have been revealed. For instance, with choline as counterion two discontinuous cubic phases extending over large concentration intervals occur up to $m = 18$. The sequence of the subsequent mesophases towards higher concentrations was confirmed to be $H_1$–$V_1$–$L_\alpha$, although the existence of an intermediate phase between $H_1$ and $V_1$ cannot be excluded. In contrast to the alkali soaps, the $V_1$ phase is formed also by long-chain members of the choline series, while the domain of $L_\alpha$ is relatively small. The use of choline as counterion in fatty acid soaps apparently promotes mesophases of high curvatures. As evidenced by the presented X-ray data, this behaviour can be ascribed to comparatively large headgroup areas originating from the bulky and highly dissociated choline ion. Another essential feature of the obtained phase diagrams is the very low Krafft boundary of ChC*m* surfactants even at high concentrations. For instance, ChC12 shows no Krafft phenomenon down to 0 °C up to 93 wt% ChC12 in water. By contrast, the corresponding sodium and potassium homologues require, at similar concentrations, far more than 100 °C to form liquid crystals.[15]

The reported phase diagrams further emphasize the potential of choline fatty acid soaps as promising alternatives to common anionic surfactants due to their extraordinary water solubility up to high concentrations and their inherent biocompatibility.

 This journal is © The Royal Society of Chemistry 2011

View Article Online

Published on 29 June 2011. Downloaded by Universitaetsbibliothek Regensburg on 21/07/2016 07:10:17.

## Experimental

### Materials and sample preparation

Choline soaps were synthesized and purified as described previously.[1] The resulting white crystalline powders were dried for at least two days in a desiccator and then stored in a nitrogen glove box.

Lyotropic liquid crystals were obtained by weighing the appropriate surfactant amount into glass ampoules of 1 cm diameter under $N_2$ atmosphere in order to gain exact concentrations and to prevent water absorption, given that neat choline soaps are hygroscopic. Subsequently, Millipore water was added such that the final total sample mass was about 0.3 g. Afterwards, the ampoules were immediately flame sealed. Adequate mixing was achieved by repeated centrifugation at around 5000 rpm for a minimum of two days at 40 °C. The homogenized samples were kept at 25 °C in a thermostat for at least 48 hours to allow for equilibration. To further ensure that thermodynamic equilibrium was in fact reached, samples were checked regularly over a period ranging from two days up to two years.

### Methods

**Penetration scan.** Penetration scan studies were conducted on a Leitz Orthoplan polarizing microscope (Wetzlar, Germany) equipped with a JVC digital camera (TK-C130) and a Linkham hot stage comprising a TMS90 temperature controller (±0.5 °C) and a CS196 cooling system. Images were recorded at a magnification of 100×. The heating or cooling rate was in all cases 10 °C $min^{-1}$. Transition temperatures on cooling were found to be up to 4 °C lower than on heating. Penetration scans were performed by trapping a small amount of dry substance between microscopy slides. Subsequently, a drop of water was added at the border of the sample, which then slowly diffused towards the centre. Distinct rings appeared along the surfactant–water concentration gradient showing the distinct mesophases, which in turn can be identified by their characteristic optical textures.[36,71] In addition, by slightly pushing the sample, relative viscosities can be estimated and used as further evidence for phase identification.

**Phase diagrams.** Concentration- and temperature-dependent mappings of the phase diagrams were first done by visual observation between crossed polarizers in steps of 2.5 wt% and 2–5 °C. Afterwards, steps were refined near the phase boundaries. The temperature of the samples was controlled by placing tubes in a water bath with an accuracy of ±0.1 °C. Specimens were investigated over a temperature range of 0–90 °C with a heating rate of about 1–2 °C per hour. Phase changes were detected by direct visual inspection of the samples between crossed polarizers. Cubic phases can be distinguished by their optical isotropy, transparency, and extremely high viscosity, while the hexagonal phase is for example featured by high viscosity, transparency and optical anisotropy. The phase boundary between the micellar solution $L_1$ and the discontinuous cubic phase $I_1$ could be easily recognized by a sudden increase of viscosity. Samples were repeatedly checked over extended periods of time (from 2 days up to 2 years). No remarkable changes with time could be discerned except for minor differences within the two-phase regions in some cases. The good agreement over this long time period indicates on the one hand that an ageing time of about 48–82 hours is already sufficient to achieve thermodynamic equilibrium and, on the other hand, that the samples are long-term stable.

**Krafft points.** The Krafft boundary within the $L_1$ phase was determined by turbidity measurements using a custom-designed automated setup built in-house.[22,72] Samples were placed in a computer-controlled thermostat and, if necessary, cooled until precipitation occurred. Turbidity was monitored by detecting the transmitted light supplied by a LED with a light-dependent resistor (LDR). The clearing temperature obtained by heating with a rate of 1 °C per hour was taken as the Krafft temperature.

**Density measurements.** In order to be able to evaluate the molecular volume of the surfactants, the densities ($\rho$) of aqueous ChC*m* solutions were determined at 25 °C for concentrations between 1 and 20 wt% using a vibrating tube densimeter (Anton Paar DMA 60). The instrument was calibrated by measuring purified dry nitrogen and water.

**Small-angle X-ray scattering.** SAXS measurements were performed on three different setups, due to limited availabilities and distinct specific demands such as the variation of detectable scattering angles, control of temperature, or the recording of two-dimensional X-ray patterns. Detailed information on the utilized SAXS instruments and on which samples were measured on each instrument is given in the ESI†. Spectra were not corrected for the empty cell scattering, since subtraction produced negative data in some instances due to temperature-induced transmission changes. However, absolute intensities are not required, as all SAXS data were analyzed crystallographically. Measured intensities are outlined as a function of the scattering vector $q$ which is defined as $q = 4\pi/\lambda \sin(\theta/2)$, where $\theta$ is the scattering angle and $\lambda$ the wavelength of the X-rays.

### Calculations

To calculate the length or radius of the lipophilic part $r_L$ and the effective cross-sectional area at the polar–nonpolar interface $a_S$ from the X-ray data, the volume fraction of the surfactant $\Phi_S$ and of the lipophilic part $\Phi_L$ are required. $\Phi_S$ is given by eqn (2), wherein $c$ denotes the weight fraction of surfactant and $\rho_{Surf}$ and $\rho_W$ are the densities of surfactant and water ($\rho_W$ = 997.1 g $L^{-1}$), respectively. Values for $\rho_{Surf}$ were obtained by extrapolating the densities measured for samples of different concentrations to 100% surfactant (see Table 4).

$$\Phi_s = \left(1 + \frac{\rho_{surf}(1-c)}{\rho_{w^c}}\right)^{-1} \quad (2)$$

Based thereon, $\Phi_L$ can be calculated according to eqn (3) where $V_S$ and $V_L$ designate the volume of surfactant and the lipophilic part, respectively.

$$\Phi_L = \frac{V_L}{V_s}\Phi_s \quad (3)$$

From the density measurements, the molar volume of surfactant and thus the volume of one surfactant molecule $V_S$ can be

View Article Online

Published on 29 June 2011. Downloaded by Universitaetsbibliothek Regensburg on 21/07/2016 07:10:17.

**Table 4** Density $\rho_{Surf}$ and volume $V_S$ of one surfactant molecule of ChC*m* salts with $m = 12$–18 at 25 °C. The volume of the lipophilic part $V_L$ and the length of the fully extended alkyl chains $l_{max}$ were calculated according to the expression introduced by Tanford[62]

| | $\rho_{Surf}$/g L$^{-1}$ | $V_S$/Å$^3$ | $V_L$/Å$^3$ | $l_{max}$/Å |
|---|---|---|---|---|
| ChC12 | 979.0 | 515 | 323 | 15.4 |
| ChC14 | 968.9 | 568 | 377 | 17.9 |
| ChC16 | 956.4 | 624 | 431 | 20.5 |
| ChC18 | 947.8 | 679 | 485 | 23.0 |

derived (Table 4). The volume of the paraffinic chains $V_L$ can in turn be estimated by using the known densities of corresponding alkanes or *via* the expression of Tanford.[62] In order to allow for a comparison with the experimentally determined lipophilic radii, Table 4 further includes the maximum (fully extended) lengths of the respective alkyl chains, which can also be calculated by the expression of Tanford.[62]

With the interlayer spacing $d$, given by the position of the first scattering peak ($d = 2\pi/q$), the radius of the lipophilic part $r_L$ and, subsequently, the cross-sectional area $a_S$ at the polar–nonpolar interface in hexagonal phases can be obtained as follows:[18]

$$r_L = d\left(\frac{2\Phi_L}{\sqrt{3\pi}}\right)^{1/2} \quad (4)$$

$$a_s = \frac{2V_L}{r_L} \quad (5)$$

For lamellar phases, the half-thickness of the lipophilic bilayer $r_L$ and the cross-sectional area $a_S$ are defined as expressed by eqn (6) and (7).[18]

$$r_L = \frac{d\Phi_L}{2} \quad (6)$$

$$a_s = \frac{V_L}{r_L} \quad (7)$$

The length of one surfactant molecule $r_S$ can finally be calculated by exchanging the lipophilic volume fraction for the surfactant volume fraction in eqn (4) and (6).

## Acknowledgements

We are grateful to Gabriele Wienskohl from the Max-Planck institute of Golm, Germany, and to Olivier Spalla from the CEA Saclay, France, for their support regarding the X-ray measurements. We are further thankful to Conxita Solans from the Institute for Advanced Chemistry of Catalonia, CSIC, Barcelona, Spain for fruitful discussions.

## Notes and references

1 R. Klein, D. Touraud and W. Kunz, *Green Chem.*, 2008, **10**, 433–435.
2 J. W. McBain and W. W. Lee, *Oil Soap (Chicago)*, 1943, **20**, 17–25.
3 R. Zana, *Langmuir*, 2004, **20**, 5666–5668.
4 R. Moberg, F. Boekman, O. Bohman and H. O. G. Siegbahn, *J. Am. Chem. Soc.*, 1991, **113**, 3663–3667.
5 E. Kutluay, B. Roux and L. Heginbotham, *Biophys. J.*, 2005, **88**, 1018–1029.
6 V. B. Luzhkov and J. Aqvist, *FEBS Lett.*, 2001, **495**, 191–196.
7 M. E. O'Leary and R. Horn, *J. Gen. Physiol.*, 1994, **104**, 507–522.
8 S. H. Zeisel and J. K. Blusztajn, *Annu. Rev. Nutr.*, 1994, **14**, 269–296.
9 J. K. Blusztajn, *Science*, 1998, **281**, 794–795.
10 J. K. Blusztajn and R. J. Wurtman, *Science*, 1983, **221**, 614–620.
11 R. Klein, M. Kellermeier, M. Drechsler, D. Touraud and W. Kunz, *Colloids Surf., A*, 2009, **338**, 129–134.
12 S. T. Hyde, Z. Blum, T. Landh, S. Lidin, B. W. Ninham, S. Andersson and K. Larsson, *The Language of Shape*, Elsevier, Amsterdam, 1996.
13 J. W. McBain and W. C. Sierichs, *J. Am. Oil Chem. Soc.*, 1948, **25**, 221–225.
14 R. D. Vold, R. Reivere and J. W. McBain, *J. Am. Chem. Soc.*, 1941, **63**, 1293–1296.
15 C. Madelmont and R. Perron, *Colloid Polym. Sci.*, 1976, **254**, 581–595.
16 V. Luzzati, H. Mustacchi and A. Skoulios, *Nature*, 1957, **180**, 600–601.
17 V. Luzzati, H. Mustacchi and A. Skoulios, *Meml. Serv. Chim. Etat*, 1957, **41**, 339–340, 337-339, discussion.
18 V. Luzzati, H. Mustacchi, A. Skoulios and F. Husson, *Acta Crystallogr.*, 1960, **13**, 660–667.
19 F. Husson, H. Mustacchi and V. Luzzati, *Acta Crystallogr.*, 1960, **13**, 668–677.
20 V. Luzzati and F. Husson, *J. Cell Biol.*, 1962, **12**, 207–219.
21 V. Luzzati, A. Tardieu, T. Gulik-Krzywicki, E. Rivas and F. Reiss-Husson, *Nature*, 1968, **220**, 485–488.
22 D. M. Small, *Handbook of Lipid Research 4: The Physical Chemistry of Lipids*, Plenum Press, New York, 1986.
23 F. Reiss-Husson and V. Luzzati, *J. Colloid Interface Sci.*, 1966, **21**, 534–546.
24 R. M. Clapperton, R. H. Ottewill, A. R. Rennie and B. T. Ingram, *Colloid Polym. Sci.*, 1999, **277**, 15–24.
25 S. Karlsson, R. Friman, S. Backlund and R. Eriksson, *Tenside, Surfactants, Deterg.*, 2004, **41**, 72–77.
26 M. Jansson, A. Joensson, P. Li and P. Stilbs, *Colloids Surf.*, 1991, **59**, 387–397.
27 K. Fontell, *Colloid Polym. Sci.*, 1990, **268**, 264–285.
28 G. Lindblom and L. Rilfors, *Biochim. Biophys. Acta, Rev. Biomembr.*, 1989, **988**, 221–256.
29 H. Hagslaett, O. Soederman and B. Joensson, *Langmuir*, 1994, **10**, 2177–2187.
30 E. S. Blackmore and G. J. T. Tiddy, *J. Chem. Soc., Faraday Trans. 2*, 1988, **84**, 1115–1127.
31 D. J. Mitchell, G. J. T. Tiddy, L. Waring, T. Bostock and M. P. McDonald, *J. Chem. Soc., Faraday Trans. 1*, 1983, **79**, 975–1000.
32 P. Sakya, J. M. Seddon, R. H. Templer, R. J. Mirkin and G. J. T. Tiddy, *Langmuir*, 1997, **13**, 3706–3714.
33 X. Li and H. Kunieda, *J. Colloid Interface Sci.*, 2000, **231**, 143–151.
34 K. Watanabe, Y. Nakama, T. Yanaki, C. Thunig, K. Horbachek and H. Hoffmann, *Langmuir*, 2004, **20**, 2607–2613.
35 A. S. C. Lawrence, *Mol. Cryst. Liq. Cryst.*, 1969, **7**, 1–57.
36 F. B. Rosevear, *J. Am. Oil Chem. Soc.*, 1954, **31**, 628–639.
37 J. M. Vincent and A. Skoulios, *Compt. Rend.*, 1964, **258**, 1229–1232.
38 S. Hassan, W. Rowe and G. J. T. Tiddy, in *Handb. Appl. Surf. Colloid Chem*, ed. K. Holmberg, John Wiley & Sons Ltd., Chichester, 2002, vol. 1, pp. 465–508.
39 J. R. Kanicky, A. F. Poniatowski, N. R. Mehta and D. O. Shah, *Langmuir*, 2000, **16**, 172–177.
40 J. R. Kanicky and D. O. Shah, *J. Colloid Interface Sci.*, 2002, **256**, 201–207.
41 J. R. Kanicky and D. O. Shah, *Langmuir*, 2003, **19**, 2034–2038.
42 J. N. Israelachvilli, D. J. Mitchell and B. W. Ninham, *J. Chem. Soc., Faraday Trans. 2*, 1976, **72**, 1525–1568.
43 D. J. Mitchell and B. W. Ninham, *J. Chem. Soc., Faraday Trans. 1*, 1981, **77**, 601–629.
44 K. Rendall, G. J. T. Tiddy and M. A. Trevethan, *J. Chem. Soc., Faraday Trans. 1*, 1983, **79**, 637–649.
45 W. Kunz, *Curr. Opin. Colloid Interface Sci.*, 2010, **15**, 34–39.
46 T. Zemb, L. Belloni, M. Dubois, A. Aroti and E. Leontidis, *Curr. Opin. Colloid Interface Sci.*, 2004, **9**, 74–80.
47 R. R. Balmbra, J. S. Clunie and J. F. Goodman, *Nature*, 1969, **222**, 1159–1160.
48 M. Clerc, *J. Phys. II*, 1996, **6**, 961–968.

 This journal is © The Royal Society of Chemistry 2011

View Article Online


49 X. Zeng, Y. Liu and M. Imperor-Clerc, *J. Phys. Chem. B*, 2007, **111**, 5174–5179.
50 S.-C. Mau and D. A. Huse, *Phys. Rev. E: Stat. Phys., Plasmas, Fluids, Relat. Interdiscip. Top.*, 1999, **59**, 4396–4401.
51 A. Tardieu and V. Luzzati, *Biochim. Biophys. Acta, Biomembr.*, 1970, **219**, 11–17.
52 P. Mariani, V. Luzzati and H. Delacroix, *J. Mol. Biol.*, 1988, **204**, 165–189.
53 P. O. Eriksson, G. Lindblom and G. Arvidson, *J. Phys. Chem.*, 1987, **91**, 846–853.
54 G. Arvidson, I. Brentel, A. Khan, G. Lindblom and K. Fontell, *Eur. J. Biochem.*, 1985, **152**, 753–759.
55 A. Tardieu, V. Luzzati and F. C. Reman, *J. Mol. Biol.*, 1973, **75**, 711–733.
56 K. Fontell, K. K. Fox and E. Hansson, *Mol. Cryst. Liq. Cryst., Lett. Sect.*, 1985, **1**, 9–17.
57 R. Vargas, P. Mariani, A. Gulik and V. Luzzati, *J. Mol. Biol.*, 1992, **225**, 137–145.
58 H. Delacroix, T. Gulik-Krzywicki, P. Mariani and V. Luzzati, *J. Mol. Biol.*, 1993, **229**, 526–539.
59 J. Charvolin and J. F. Sadoc, *J. Phys. Chem.*, 1988, **92**, 5787–5792.
60 Y. Rancon and J. Charvolin, *J. Phys. Chem.*, 1988, **92**, 2646–2651.
61 P. Mariani, L. Q. Amaral, L. Saturni and H. Delacroix, *J. Phys. II*, 1994, **4**, 1393–1416.
62 C. Tanford, *J. Phys. Chem.*, 1972, **76**, 3020–3024.
63 B. Gallot and A. Skoulios, *Kolloid. Z. Z. Polym.*, 1966, **208**, 37–43.
64 H. Hagslaett, O. Soederman and B. Joensson, *Liq. Cryst.*, 1992, **12**, 667–688.
65 P. Saludjian and F. Reiss-Husson, *Proc. Natl. Acad. Sci. U. S. A.*, 1980, **77**, 6991–6995.
66 S. Piotto, *Origins Life Evol. Biospheres*, 2004, **34**, 123–132.
67 S. Andersson, S. T. Hyde, K. Larsson and S. Lidin, *Chem. Rev.*, 1988, **88**, 221–242.
68 K. Larsson and F. Tiberg, *Curr. Opin. Colloid Interface Sci.*, 2005, **9**, 365–369.
69 V. Luzzati and F. R. Husson, *Nature*, 1966, **210**, 1351–1352.
70 O. Söderman, *Curr. Opin. Colloid Interface Sci.*, 2004, **9**, 154–157.
71 F. B. Rosevear, *J. Soc. Cosmet. Chem.*, 1968, **19**, 581–594.
72 S. Schroedle, R. Buchner and W. Kunz, *Fluid Phase Equilib.*, 2004, **216**, 175–182.


Published on 29 June 2011. Downloaded by Universitaetsbibliothek Regensburg on 21/07/2016 07:10:17.